NUMERICAL STUDY ON BUBBLE MERGER IN A HEATED SYMMETRIC MICROFLUIDIC T-JUNCTION

Weiyu LIU[a], Zhenhua JIANG[b], Baoyu YANG[b], Zhe YAN[b*], and Zhenhai PAN[c]

[a] Institute of Translational Medicine, Shanghai Jiao Tong University, Shanghai 200240, China

[b] Shanghai Institute of Technical Physics, Chinese Academy of Sciences, Shanghai 200083, China

[c] School of Mechanical Engineering, Shanghai Institute of Technology, Shanghai 201418, China

[*] Corresponding author; E-mail: yanzhe@mail.sitp.ac.cn

In this work, the bubble merger process in a heated symmetric microfluidic T-junction is numerically studied with the variations of heat flux and seed bubble volume. Detailed bubble behaviors and phase change heat transfer characteristics are revealed. Results show that the bubble experiences slipping and colliding merger regimes at small and large seed bubble volumes, respectively. The bubble grows faster at large heat flux and seed bubble volume. Obvious peak in evaporation rate during the bubble merger can be seen. The bubble behaviors significantly affect the phase change heat transfer. The asymmetry of bubble behaviors under slipping merger regime leads to the heat transfer difference between two main channel walls. Besides, the squeezing effect during bubble merger could promote the heat transfer. Generally, the heat transfer enhancement becomes stronger as the heat flux and seed bubble volume are increased. The present study's findings could improve the understanding of bubble behaviors and transport details in microfluidic T-junction structures.

Key words*: Microfluidic T-junction, bubble merger, phase change, heat transfer, VOF method*

1. Introduction

In recent years, microfluidic devices have been widely used to various fields including biomedical engineering, pharmaceutical industry, chemical engineering, and electronics cooling [1, 2]. Among various cooling technologies explored, flow boiling in confined spaces has received considerable attentions due to its outstanding heat transfer performance [3-5]. Physically, the performance of two-phase heat dissipation is related to the bubble behaviors [6]. It is of crucial importance to reveal the complex bubble behaviors in the confined spaces, so as to efficiently design and optimize the two-phase microfluidic devices.

As a common physical phenomenon, the bubble merger (also known as bubble coalescence) behaviors exist in both nature and industry [7-9], especially for the industrial boiling system [10-12]. Recently, to help developing the high-performance two-phase microfluidic devices for electronics cooling, some researchers have placed emphasis on bubble merger behaviors in confined straight structure under phase change/flow boiling condition. Lu *et al*. [13] developed visualization experiment to study the bubble merger behaviors in a narrow vertical channel. The relationship between flow

pattern transition and bubble merger was revealed. The microlayer was found to play an important role in both bubble behaviors and boiling heat transfer. Pattamatta *et al*. [14] carried out both experiments and simulations on the merger of FC-72 Taylor-bubble in a heated square minichannel. The detailed parametric studies showed that the merger period is reduced for unequal bubbles. Reynolds number and wall superheat could influence wall heat transfer more significantly than others factors. Liu *et al*. [15] simulated the merger of multiple evaporating bubbles in microchannel on the basis of CLSVOF method. Saturated temperature, wall heat flux, and mass flux were set as influencing parameters. Results showed that the evaporation rate kept at higher level during the sliding and merger stages. Bhuva *et al*. [16] numerically investigated the bubble merger during flow boiling in straight and raccoon microchannels. Force analysis on bubble was performed, and it was found that the negative trend existed between the pressure forces of the leading and trailing bubbles. Li *et al*. [17] focused on the flow boiling of self-rewetting fluid and numerically studied the related bubble merger in microchannel. Both the merger processes of two-bubbles and three-bubbles were simulated. The optimum heat transfer enhancement occurred on the merger of two-bubbles in x-direction. Very recently, Zhang *et al*. [18] developed the self-programmed solver and numerically studied the bubble merger during flow boiling in rectangular microchannels with the consideration of conjugate heat transfer. Three bubble merger stages including bridging, retraction, and bubble contraction were found. The heat transfer enhancement was analyzed for each merger stage. Above studies have shown that there exists close relationship between the bubble dynamics and performance of microfluidic devices.

Branching structures can control the fluid flow distribution and manipulate the bubble behaviors (breakup and merger). Compared with the bubble merger, the bubble breakup in branching structures has obtained more attentions. Zhang *et al*. [19] numerically investigated the bubble breakup in double T-type microchannel. By varying the capillary number and bubble length, five different breakup regimes can be observed. Wang *et al*. [20] focused on bubble breakup with partly obstruction in T-shaped branching channels. Based on the visualization experiments, the detailed evolution of bubble neck width was presented and two breakup stages were summarized. Sheng *et al*. [21] experimentally explored the bubble breakup during the generation process in T-shaped branching microchannel. Under the higher viscosity, the generation of satellite bubbles can be seen. The mathematical model was proposed for the prediction of the bubble length. The bubble merger could be considered as the reverse process of bubble breakup. Yang *et al*. [22] conducted study on coalescence of microbubble in microfluidic T-junction. Three various bubble behaviors including non-coalescence, probabilistic coalescence, and absolute coalescence were found. The confined effect could promote the coalescence behavior. The boundary between the coalescence and non-coalescence was described. Wu *et al*. [23] reported their experiment and simulation investigations about the bubble merger in square microfluidic T-junction with the size of 400 μm. Various coalescence regimes were presented by changing the capillary number and bubble size. The coalescence efficiency was proposed to evaluate the coalescence behaviors. Above studies have shown the important role of branching structures. Besides, the complex bubble dynamics are involved in the process of bubble passing through branching structures.

It is summarized that, compared with the bubble merger behaviors in heated confined straight structures, few studies have focused on the bubble merger in heated confined branching structures while these structures have shown promising potentials in the development of high-performance cooling devices [24, 25]. The objective of present work is to reveal the bubble behaviors and phase

change heat transfer characteristics involved in bubble merger process. The typical microfluidic T-junction is selected as research object. Specifically, two key influencing parameters (heat flux and seed bubble volume) are considered and the related physical mechanisms are revealed thoroughly.

2. Problem description and development of numerical model

2.1. Problem description

Figure 1 shows the diagrammatic sketch for bubble merger in heated symmetric microfluidic T-junction and the definition of various walls. Only half domain is considered in simulations due to the symmetric characteristics. The microfluidic T-junction has the square cross-section, where the width (W) is 100 μm. On the basis of geometric characteristics, the microfluidic T-junction can be divided into upstream branching channel (BC) and downstream main channel (MC). The upstream branching channel (BC) has three various walls, namely the inner wall (BC-I), outer wall (BC-O), and top wall (BC-T). Unlike the branching channel, the downstream main channel (MC) has two various walls, namely the outer wall (BC-O) and top wall (BC-T). According to the boundary condition, the microfluidic T-junction consists of two regions (adiabatic region and heated region) and the present study mainly concentrates on physical phenomenon phenomena in heated region. The length for heated BC-O and MC-O are all 10 W.

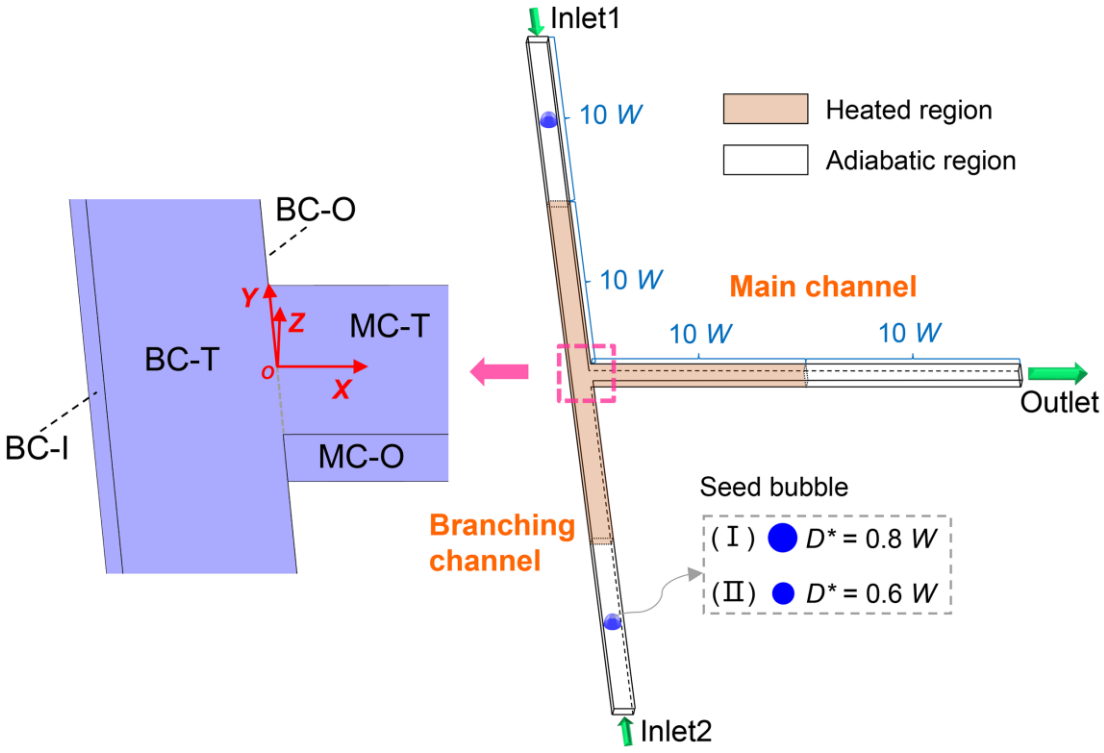

Figure 1. The diagrammatic sketch for bubble merger in heated symmetric microfluidic T-junction and the definition of various walls

The boundary condition for inlet is velocity inlet, and all the simulations are performed under the same inlet Reynolds number (Re) of 300. Therefore, the flow state in microfluidic T-junction belongs to the laminar flow. The boundary condition for outlet is pressure outlet, with the atmospheric value. In this numerical study, the seed bubble strategy is employed [26]. The seed bubbles are added to

computational domain once the single-phase flow fields reach the steady state. The seed bubble volume is set as variable, which is characterized by the dimensionless bubble diameter D^* (D/W). Two different seed bubble volumes (D^* = 0.6 and D^* = 0.8) are considered. The heat flux q imposed on the walls of heated region is set as another variable. Two heat fluxes (q = 2000 Wm^{-2} and q = 8000 Wm^{-2}) are taken into account. This study focuses on one working medium, namely the saturated HFE-7100, and its physical properties are listed in tab. 1.

Table 1. Physical properties of HFE-7100 medium [27]

Properties	Liquid	Vapor
σ [Nm^{-1}]	0.0136	0.0136
μ [Pa·s]	3.56×10^{-4}	1.11×10^{-5}
ρ [Kgm^{-3}]	1425	5.15
λ [$Wm^{-1}K^{-1}$]	0.0618	0.0103
c_p [$KJKg^{-1}K^{-1}$]	1.430	0.900
h_{fg} [$KJKg^{-1}$]	117.8	117.8

2.2. Numerical modelling

The volume of fluid (VOF) method with the color function (C) is utilized to distinguish various phases [28, 29]. Excellent mass conservation can be achieved by employing VOF method. The relationship between color function and different phases is:

$$\begin{cases} C = 0, & \text{without tracked phase} \\ 0 < C < 1, & \text{interface} \\ C = 1, & \text{filled with tracked phase} \end{cases} \tag{1}$$

The conservation equations are:
Continuity equation:

$$\frac{\partial(C_i\rho_i)}{\partial t} + \nabla\cdot(C_i\rho_i\vec{U}) = S_{m,i} \tag{2}$$

Momentum equation:

$$\frac{\partial(\rho\vec{U})}{\partial t} + \nabla(\rho\vec{U}\cdot\vec{U}) = -\nabla P + \nabla(\mu(\nabla\vec{U} + \nabla\vec{U}^T)) + \overrightarrow{F_S} \tag{3}$$

Energy equation:

$$\frac{\partial(\rho c_p T)}{\partial t} + \nabla(\rho c_p T\vec{U}) = \nabla\cdot(\lambda\nabla T) + S_h \tag{4}$$

where S_h reprents the energy source term, and it is the sum of latent heat source term and sensible heat source term:

$$S_h = S_{h,la} + S_{h,s} \tag{5}$$

The continuum surface force model is responsible for the calculation of surface tension effect [30]:

$$\overrightarrow{F_s} = \sigma\kappa\delta_s\vec{n} = -\sigma\nabla\cdot\left(\frac{\nabla C}{|\nabla C|}\right)|\nabla C| \tag{6}$$

where κ and σ respectively represent the surface tension coefficient and the interface curvature. One challenge occurs in the employment of VOF-CSF model is the non-physical velocity. We employ the self-proposed moving reference frame method to suppress the non-physical velocity [31]. The physics-based calculation of phase change is of great importance. The self-proposed saturated-interface-volume (SIV) model is employed to be responsible for the phase change calculation [32], which enables the relatively low computational cost while keeping the calculation accuracy. Besides, the calculation stability this model is excellent. The interfacial temperature always keeps at saturated state for each iteration. The latent heat energy source ($S_{h,la}$) added on each cell is calculated by:

$$S_{h,la} = \frac{C_l\rho_l c_{pl}(T_{sat}-T) + C_v\rho_v c_{pv}(T_{sat}-T)}{\Delta t} \tag{7}$$

Besides, the above-mentioned sensible heat energy source can be obtained by:

$$S_{h,s} = S_{m,l}c_{pl}(T-T_{ref}) + S_{m,v}c_{pv}(T-T_{ref}) \tag{8}$$

The SIV phase change model is implemented by the ANSYS FLUENT package with self-developed User-Defined Functions (UDFs). In simulations, the pressure-velocity coupling employs the PISO algorithm. The volume-fraction discretization is implemented with the Geo-Reconstruct method.

The mesh configuration and independence test are respectively shown in fig. 2(a) and fig. 2(b). As can be seen, the boundary layer mesh is configured, so as to get the more precise results [33]. Mesh independence test based on the dimensionless bubble volume has been performed with the total cell number ranging between 1514844 and 5340824. Taking the computation accuracy and cost into account, the adopted cell number is 3820684.

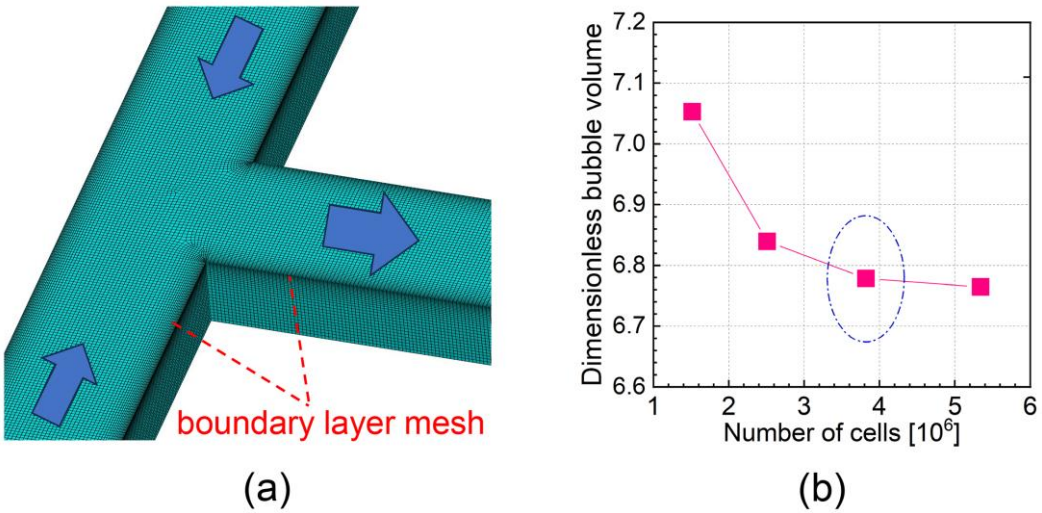

Figure 2. Mesh configuration (a) and independence test (b)

2.3. Model validation

To verify the accuracy of developed numerical model, the experimental results in literature [14] are used, where two unequal bubbles merge in the straight minichannel under the flow boiling condition. The square channel has the size of 2 mm. The top wall of channel owns the superheat of 2 K while the side and bottom walls are adiabatic. The working medium is saturated FC-72. The inlet Reynolds number is 269. Figure 3(a) shows the equivalent bubble diameter as a function of time. The average and maximum deviations in equivalent bubble diameter between the simulation and experiment are 1.48% and 3.32%, respectively. Figure 3(b) shows the bubble shapes at some typical moments. Notably, the simulated results are consistent with the experimental results, thus indicating the accuracy of developed numerical model.

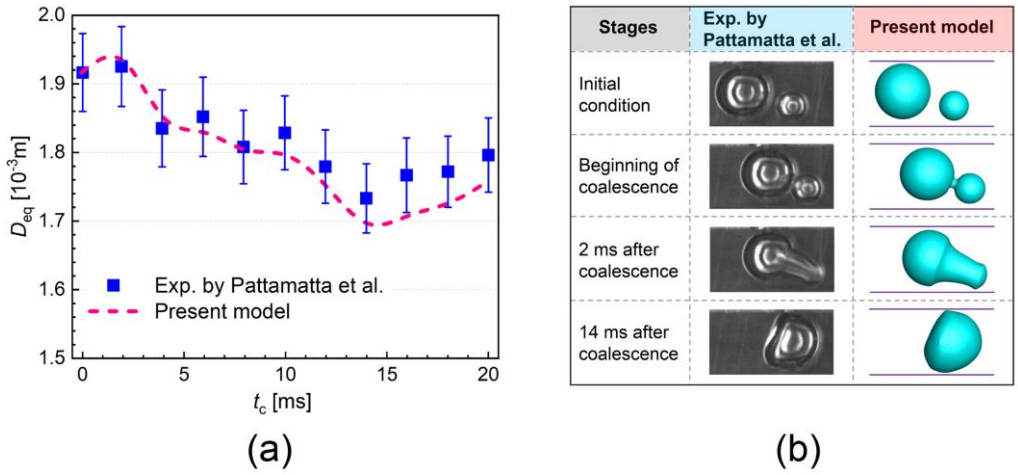

Figure 3. Validation of the developed numerical model by the experimental results from Pattamatta *et al.* [14]: (a) equivalent bubble diameter and (b) bubble shape

3. Results and discussion

3.1. Bubble merger process

Figure 4 presents the bubble shapes and velocity fields during the merger process. At low heat flux of 2000 Wm^{-2} (see fig. 4(a)), the bubble grows slowly and its size is still small in bifurcating region. For the moment of bubble nose touching the boundary, obvious gap between the bubble and BC-I wall emerged, namely the bubble cannot fully obstruct the channel. After the bubble nose enters the main channel, the distance between them gradually reduces. Soon afterwards, the two bubbles touch each other and then the bubble neck starts to grow until the accomplishment of bubble merger. This merger regime belongs to the typical colliding merger [23]. During the merger process, excellent symmetry characteristics relatively to the central line of main channel can be seen. As the heat flux increases to 8000 Wm^{-2} (see fig. 4(c)), the bubble volume increases and the bubble can fully obstruct the channel. The bubble merger is still in process when the bubble nose locates at 3 *W*. In this situation, the bubble merger regime also belongs to colliding merger. For the case of small seed bubble volume ($D^* = 0.6$, see fig. 4(b)), not only the gap exists in the side of BC-I wall, but also it emerges in the side of BC-O wall. One result of interest is that, the two bubbles cannot enter the main channel at the same time. They enter the main channel in succession instead. Essentially, the transition from symmetry to asymmetry is more likely to occur in cases with small bubble sizes. In the main channel, the bubble

nose of the latter bubble touches the former bubble, inducing the merger process. This distinctive merger regime is named as the slipping merger.

Under single-phase flow, the distribution of velocity is uneven in the central plane. Due to the flow convergence, an elongated region with high velocity emerges in the main channel. Under two-phase flow, the bubble could influence the distribution of velocity. The phase change leads to bubble growth, which accelerates the downstream fluid flow. The acceleration phenomenon becomes obvious at lager heat flux and seed bubble volume.

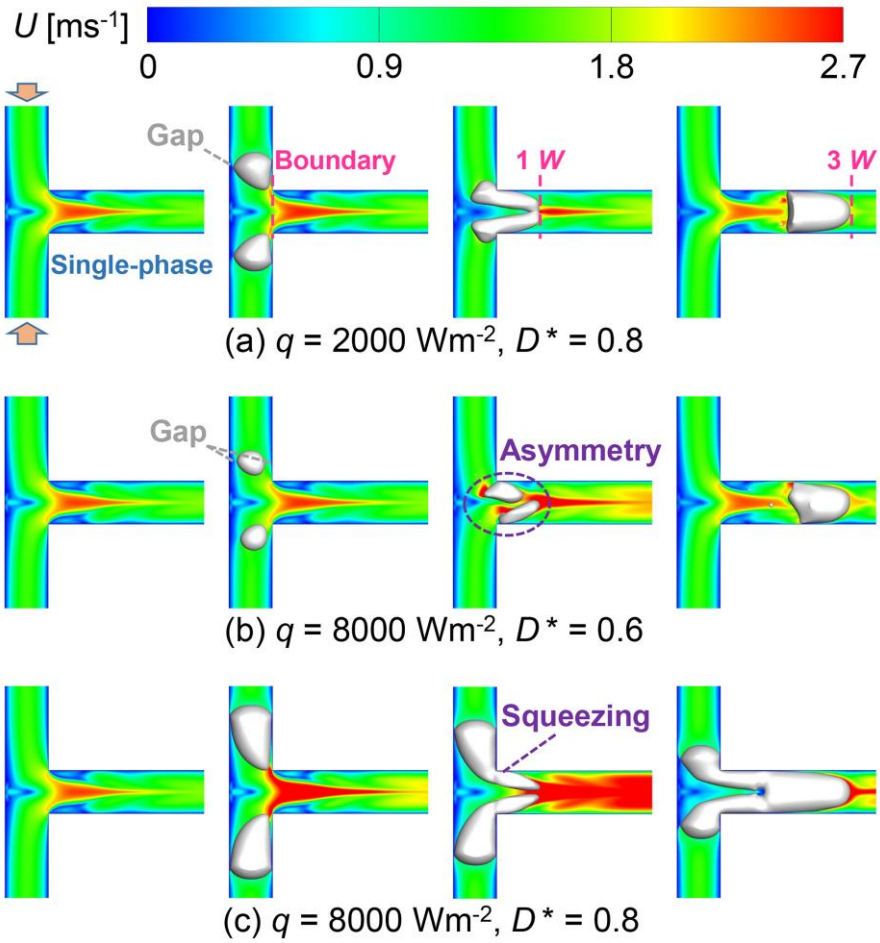

Figure 4. Bubble shapes and velocity fields during the merger process at different heat fluxes and seed bubble volumes

The evolutions of bubble volume and evaporation rate are respectively shown in figs. 5(a) and 5(b). Obviously, the bubble volume tends to increase after the bubble enters heated region. The smaller the seed bubble volume, the turning point for the bubble volume appears later. This is because that the larger bubble could touch the thermal boundary layer earlier. As the heat flux and seed bubble volume are increased, both the evaporation rate and ultimate bubble volume rise correspondingly. Obvious evaporation rate peak for all three cases an be seen. This is due to the squeezing of bubbles during the merger process, which induces the thin liquid film. The smaller bubble tends to reach its evaporation rate peak earlier. This can be attributed to the larger motion velocity occurring on the bubble with smaller initial volume.

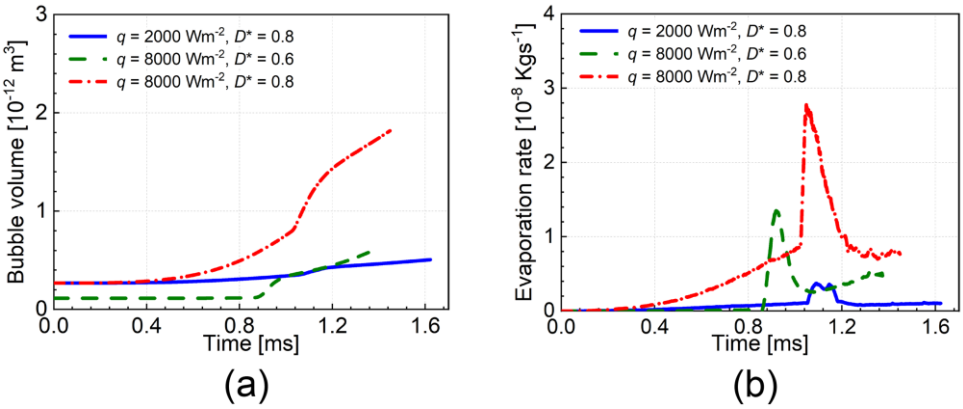

Figure 5. The evolutions of bubble volume and evaporation rate

3.2. Heat transfer characteristics

Firstly, the detailed temperature fields are analyzed, as can be seen in fig. 6. Under the single-phase case, the destruction in thermal boundary layer can be observed in central region of BC-I wall. The temperature fields for the main channel are relatively chaotic because of the complex flow path in convergence behavior. The temperature is increased with the increasing heat flux. Under the two-phase case, the evaporation process induced by the bubble could absorb the sensible heat. At the same time, the channel wall is significantly cooled. The larger bubble leads to the more significant cooling effect. During the bubble merger process, the bubble cannot touch the central region of BC-I wall. As a result, the temperature fields in this region are less affected by the bubble.

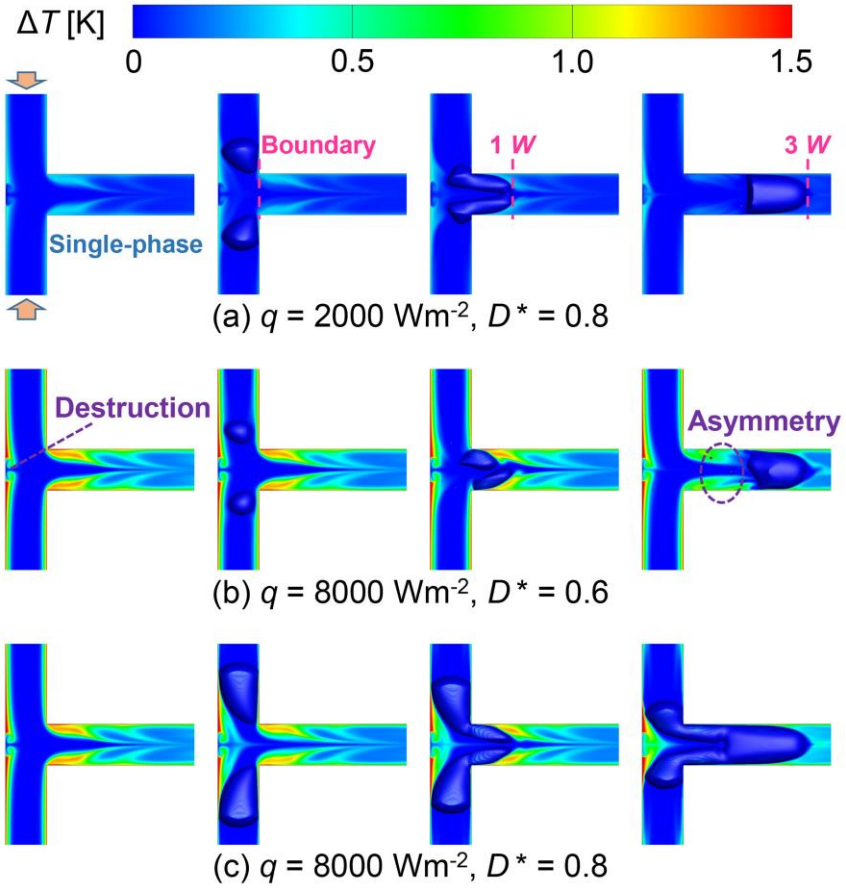

Figure 6. Temperature fields at different heat fluxes and seed bubble volumes

To facilitate the heat transfer analysis, the distribution of Nusselt number (*Nu*) for the upstream branching channel is shown in fig. 7. Three cases are taken into account, where the bubble nose respectively locates at boundary between the MC and BC (0 *W*), 1 W position of MC, 2 *W* position of MC. Single-phase heat transfer is also shown to aid in analyzing. Motivated by the convergent flow, the single-phase heat transfer in the junction region is relatively strong. For BC-I and BC-T walls, the obvious peak in Nusselt number can be seen and the influencing region for the BC-T wall is larger than that of BC-I wall. Under two-phase condition, the heat transfer is improved due to the phase change. Both the heat flux and seed bubble volume play significant roles in phase change heat transfer. The heat transfer enhancement is relatively weak at $D^* = 0.6$. In this case, the liquid film is relatively thick, and there exists relatively large thermal resistance. As the heat flux and seed bubble volume increase, the heat transfer enhancement becomes visible. Generally, the heat transfer enhancement for BC-O wall is most noticeable. Very strong heat transfer enhancement in the corner region of BC-O wall emerges when the bubble locates at 1W and 3W positions. This can be attributed to the squeezing effect during the bubble moving to main channel, which leads to the occurrence thin liquid film.

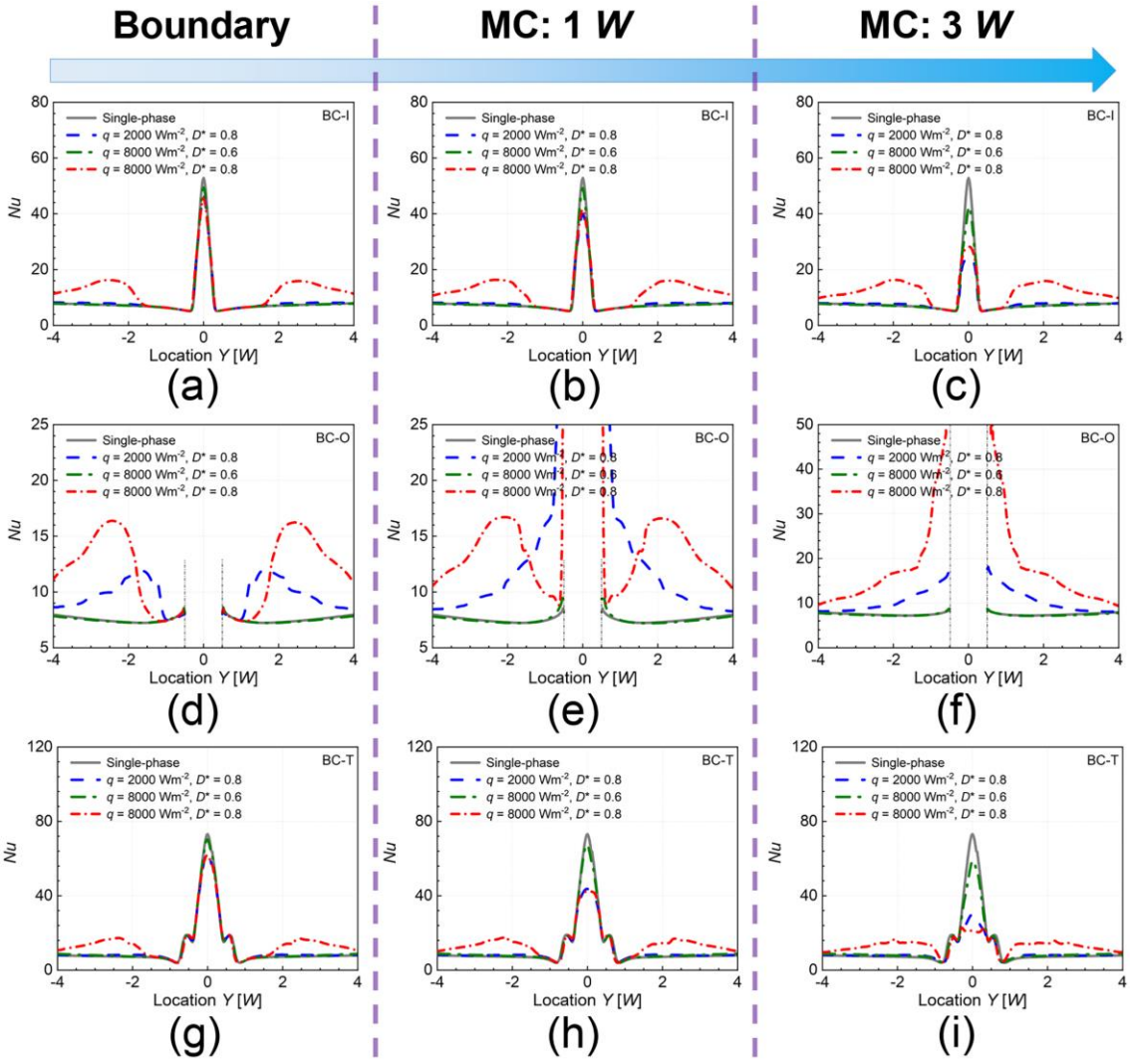

Figure 7. Distribution of Nusselt number for the upstream branching channel

The distribution of Nusselt number for the downstream main channel is shown in fig. 8, which is quite different with that of branching channel. Along the flow direction, the fluctuations (two peaks) in Nusselt number of MC-O wall can be observed. The heat transfer of MC-O wall is significantly enhanced due to the phase change and very strong heat transfer can be observed in the corner region. When the seed bubble volume is small, as can be seen in fig. 4(b), the asymmetry in bubble behaviors within the main channel occurs. As a result, the difference in heat transfer between two MC-O walls of main channel can be seen. This phenomenon becomes more obvious as the bubble moves from 1W location to 3 *W* location. The single-phase Nusselt number of MC-T wall is found to decrease along the flow direction. Interestingly, the suppression effect in heat transfer is observed with the occurrence of bubble. This is because that the bubble could change the local fluid flow, which further weakens the local convective heat transfer.

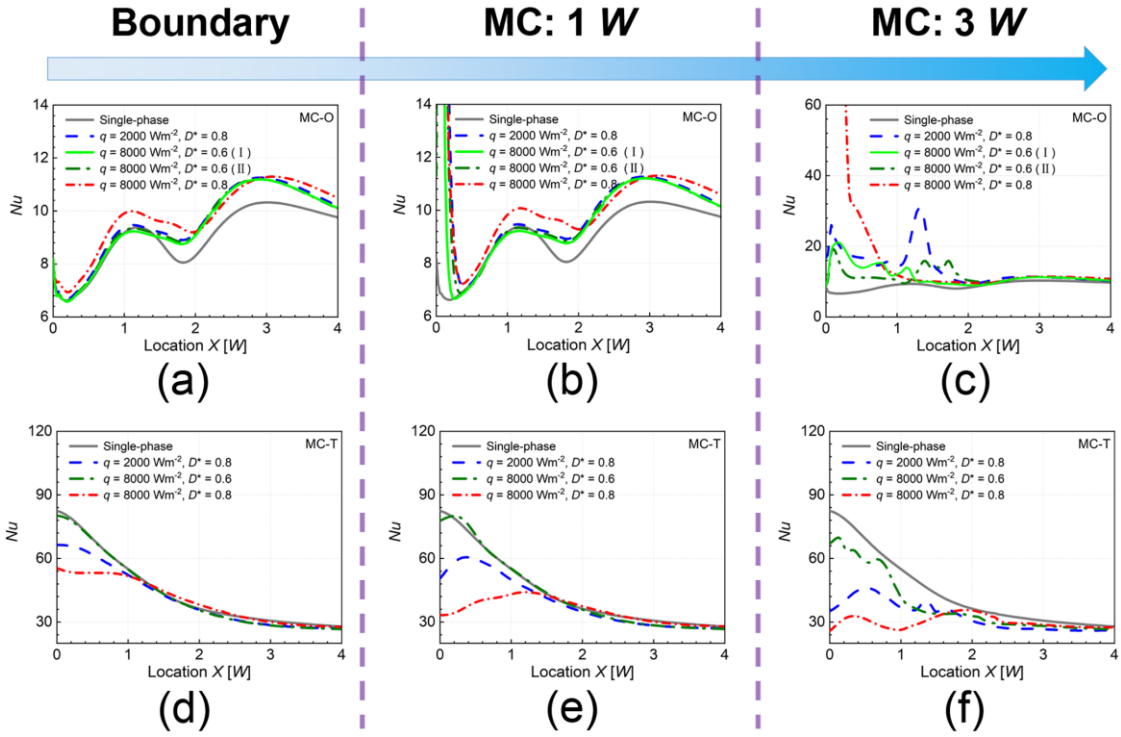

Figure 8. Distribution of Nusselt number for the downstream main channel

4. Conclusions

In this paper, the numerical study on bubble merger process in a symmetrical heated microfluidic T-junction is performed. The VOF-based numerical model is validated against experimental results in literature. Two important variables (heat flux and seed bubble volume) are considered and their influences on merger process are analyzed. Two different bubble merger regimes including slipping and colliding merger regimes are found. The bubble grows faster at larger heat flux and seed bubble volume. The squeezing effect occurs when the bubble moves from branching channel to main channel, which triggers the peak of evaporation rate and strong heat transfer enhancement. The asymmetry of bubble behaviors under slipping merger results in the heat transfer difference between two opposite main channel walls. Besides, the heat transfer suppression phenomenon is found to emerge on the main channel region. The present study provides new insights into the manipulation of bubble dynamics, which could help the design of high-performance microfluidic devices. Future

studies are encouraged to focus on asynchronous merger of two bubbles with unequal sizes, and new phenomenon as well as physical mechanism could be revealed.

Nomenclature

BC-I	-inner wall of branching channel, [-]
BC-O	-outer wall of branching channel, [-]
BC-T	-top wall of branching channel, [-]
C	-volume fraction, [-]
c_p	-specific heat capacity, [KJKg^{-1}K^{-1}]
D	-seed bubble diameter, [m]
F_s	-surface tension, [N]
h_{fg}	-latent heat [KJKg^{-1}]
MC-O	-outer wall of main channel, [-]
MC-T	-top wall of main channel, [-]
Nu	-Nusselt number, [-]
q	-wall heat flux, [Wm^{-2}]
Re	-Reynolds number, [-]
S_h	-energy source, [Wm^{-3}]
T	-temperature, [K]
Δt	-time step, [s]
U	-velocity, [ms^{-1}]
W	-width of microchannel, [m]

Greek symbols

ρ	-density, [Kgm^{-3}]
μ	-dynamic viscosity, [Pa·s]
σ	-surface tension coefficient, [Nm^{-1}]
λ	-thermal conductivity, [Wm^{-1}K^{-1}]
υ	-kinematic viscosity, [m^{2}s^{-1}]
κ	-boundary curvature, [m^{-1}]

Superscripts and subscripts

*	-dimensionless treatment

References

[1] Ma, X., *et al.*, Flow boiling frictional pressure drop inside micro/mini-channels: A new general model and experimental investigation, *Applied Thermal Engineering*, *247*. (2024), p. 123111,

[2] Anandan, S.,V. Ramalingam, Thermal management of electronics: A review of literature, *Thermal Science*, *12*. (2008), 2, pp. 5-26

[3] Tang, J., *et al.*, Enhanced heat transfer coefficient of flow boiling in microchannels through expansion areas, *International Journal of Thermal Sciences*, *177*. (2022), p. 107573

[4] Asim, M., *et al.*, Flow boiling heat transfer characteristics of low global warming potential refrigerants in a vertical mini-channel, *Thermal Science*, *26*. (2022), 1 Part A, pp. 63-76

[5] Chen, J., *et al.*, Numerical investigation on saturated boiling flow and heat transfer of mixture refrigerant in a vertical rectangular mini-channel, *Thermal Science*, *22*. (2018), 2, pp. 617-627

[6] Liu, Y., *et al.*, The suppression effect of easy-to-activate nucleation sites on the critical heat flux in pool boiling, *International Journal of Thermal Sciences*, *129*. (2018), pp. 231-237

[7] Zhang, Y., *et al.*, The effect of fluctuating pressure gradient on the coalescence of Taylor bubble, *Canadian Journal of Physics*, *99*. (2021), 7, pp. 501-512

[8] Shaw, D.B.,L. Deike, Surface bubble coalescence, *Journal of Fluid Mechanics*, *915*. (2021), p. A105

[9] Cui, P., *et al.*, Experimental study on interaction and coalescence of synchronized multiple bubbles, *Physics of Fluids*, *28*. (2016), 1, p. 012103

[10] Liu, J., *et al.*, Bubble coalescence during pool boiling with different surface characteristics, *Heat Transfer Engineering*, *45*. (2024), 4-5, pp. 360-380

[11] Mondal, K.,A. Bhattacharya, Numerical modeling of adjacent bubble interactions under the influence of induced vibrations in liquid pool using lattice Boltzmann method (LBM), *Journal*

of Applied Physics, *130*. (2021), 22, p. 224701
[12] Zhao, Z., *et al.*, Investigation of bubbles interaction and coalescence boiling in the boiling heat transfer process, *Thermal Science*, *23*. (2019), 5 Part A, pp. 2605-2611
[13] Lu, Q., *et al.*, Visual investigation on the coalescence process and the thermal-hydraulic characteristics of the two-phase interface morphology in narrow vertical channel, *International Journal of Heat and Mass Transfer*, *115*. (2017), pp. 537-550
[14] Pattamatta, A., *et al.*, A parametric study on phase change heat transfer due to Taylor-Bubble coalescence in a square minichannel, *International Journal of Heat and Mass Transfer*, *76*. (2014), pp. 16-32
[15] Liu, Q., *et al.*, Numerical study of the interactions and merge of multiple bubbles during convective boiling in micro channels, *International Communications in Heat and Mass Transfer*, *80*. (2017), pp. 10-17
[16] Bhuva, V.J., *et al.*, Effect of bubble coalescence on two-phase flow boiling heat transfer in raccoon microchannel - A numerical study, *International Journal of Heat and Mass Transfer*, *182*. (2022), p. 121943
[17] Li, W., *et al.*, Numerical investigation on bubble growth and merger in microchannel flow boiling with self-rewetting fluid, *Journal of Heat Transfer*, *143*. (2021), 6, pp. 1-10
[18] Zhang, Z., *et al.*, The bubble merger in rectangular microchannels during boiling processes based on conjugate heat transfer, *Applied Thermal Engineering*, *247*. (2024), p. 123093
[19] Zhang, Z., *et al.*, The bubble breakup process and behavior in T-type microchannels, *Physics of Fluids*, *35*. (2023), 1, p. 013319
[20] Wang, X., *et al.*, Dynamics of bubble breakup with partly obstruction in a microfluidic T-junction, *Chemical Engineering Science*, *132*. (2015), pp. 128-138
[21] Sheng, L., *et al.*, Taylor bubble generation rules in liquids with a higher viscosity in a T-junction microchannel, *Industrial & Engineering Chemistry Research*, *61*. (2022), 6, pp. 2623-2632
[22] Yang, L., *et al.*, Experimental study of microbubble coalescence in a T-junction microfluidic device, *Microfluidics and Nanofluidics*, *12*. (2011), 5, pp. 715-722
[23] Wu, Y., *et al.*, Bubble coalescence at a microfluidic T-junction convergence: from colliding to squeezing, *Microfluidics and Nanofluidics*, *16*. (2013), 1-2, pp. 275-286
[24] Zhang, J., *et al.*, Numerical investigation of heat transfer and pressure drop characteristics of flow boiling in manifold microchannels with a simple multiphase model, *International Journal of Heat and Mass Transfer*, *211*. (2023), p. 124197
[25] Wang, Y., *et al.*, Thermal management of electronic components based on hierarchical microchannels and nanofluids, *Thermal Science and Engineering Progress*, *42*. (2023), p. 101910
[26] Zong, L., *et al.*, Numerical study of seed bubble-triggered evaporation heat transfer in a single microtube, *Microfluidics and Nanofluidics*, *16*. (2013), pp. 347-360
[27] NIST, NIST Chemistry Web Book, https://doi.org/10.18434/T4D303. (2018)
[28] Bai, Y., *et al.*, Bubby behavior and heat transfer characteristics of bionic microchannels in the subcooled flow boiling process, *Numerical Heat Transfer, Part A: Applications*. (2024), pp. 1-18
[29] Dong, F., *et al.*, A novel interphase mass transfer model toward the VOF simulation of subcooled flow boiling, *Numerical Heat Transfer, Part A: Applications*, *76*. (2019), 4, pp. 220-231
[30] Brackbill., J.U., *et al.*, A continuum method for modeling surface tension, *Journal of Computational Physics*, *100*. (1992), 2, pp. 335-354
[31] Pan, Z., *et al.*, Spurious current suppression in VOF-CSF simulation of slug flow through small channels, *Numerical Heat Transfer, Part A: Applications*, *67*. (2014), 1, pp. 1-12
[32] Pan, Z., *et al.*, A saturated-interface-volume phase change model for simulating flow boiling, *International Journal of Heat and Mass Transfer*, *93*. (2016), pp. 945-956
[33] Magnini, M.,O.K. Matar, Numerical study of the impact of the channel shape on microchannel boiling heat transfer, *International Journal of Heat and Mass Transfer*, *150*. (2020), p. 119322

Submitted: 4.10.2024.
Revised: 12.12.2024.
Accepted 16.12.2024.